Preprint version

Enhancing Spacecraft Relative Motion Control through Fuzzy Inference System Interpretability

Daegyun Choi and Donghoon Kim

Abstract In-space servicing has gained significant interest for extending the mission life of spacecraft with faulty components. This involves rendezvous and proximity maneuvers for a servicing spacecraft, called a chaser, to move toward a malfunctioning satellite, called a target. A fuzzy inference system (FIS)-based control strategy for the chaser to safely approach the cooperative target was proposed while minimizing the chaser's control effort via offline training facilitated by a genetic algorithm as preliminary work. The primary focus of this work is not only to identify the reasons for the issue of the trained FIS control approach in the preliminary work, which entails a sudden change of sign in the control force trajectory, by exploiting the FIS's interpretability but also to address such issue by introducing an independent FIS for the coupled axis and retraining it. The results demonstrate that the improved FIS controller generates a smooth control force trajectory.

1 Introduction

Since the advent of spaceflight in the 20th century, a significant number of spacecraft have been launched into space. Typically, the operational lifespan of these spacecraft is dependent on their mission design. However, executing missions as planned has proven challenging due to the complexity of repairing faulty components once a spacecraft is in space, particularly if it experiences malfunctions in sensors or actuators. Recently, there has been considerable interest in in-space servicing, including activities such as refueling, upgrading, and repairing components, aimed at extending the missions of spacecraft with defective parts, thanks to advancements in space technologies, including electronics, rockets, and spacecraft. Such missions require

Daegyun Choi
University of Cincinnati, Cincinnati, OH, USA, e-mail: Daegyun.Choi@uc.edu

Donghoon Kim
University of Cincinnati, Cincinnati, OH, USA, e-mail: Donghoon.Kim@uc.edu

rendezvous and proximity operations (RPOs) of spacecraft, often referred to as a chaser, to provide service [9, 15]. When approaching a target that demands service for approaching from a different orbit, the chaser initiates a phasing process to align with the target's orbit. Then, the chaser undergoes far- and close-range rendezvous maneuvers until the relative distance decreases to around 100 m. Subsequently, the chaser conducts the final approach process to minimize the relative distance from the target, aiming for near-zero proximity. This work primarily concentrates on the final approach phase within the entire rendezvous process.

Numerous researchers have investigated several approaches for safe RPO missions. Among them, some scholars have employed the widely used artificial potential field (APF) approach, which is a collision avoidance method commonly used for autonomous robotic platforms. Based on the APF concept, various control laws, such as backstepping control [10], first-order sliding mode control [12], sub-optimal sliding mode control [2], and non-singular terminal sliding mode control [11], have been integrated to govern spacecraft during the final approach phase of RPOs. With the advancement of computing technologies, some scholars have turned to artificial intelligence (AI) or learning-based techniques to address diverse control problems and platforms, and examples include explainable AI-based spacecraft attitude control [3], decentralized ground multi-robot control for collaborative tasks [6], and collision-free navigation of aerial vehicles [4]. Notably, some studies have applied the reinforcement learning (RL) approaches [8, 13, 1] to execute spacecraft proximity operations. These investigations have assessed RL's performance in spacecraft RPO missions, particularly in terms of energy consumption. Nevertheless, RL lacks interpretability regarding both the decision-making process and resultant outputs. On the other hand, a fuzzy inference system (FIS) offers transparent and interpretable resultant outputs because the decision-making process is based on linguistic variables and If-Then rules, unlike the RL-applied controller.

In the author's previous work, one has developed an FIS-applied control strategy for the final approach of the spacecraft rendezvous and proximity operations [5] while incorporating a genetic algorithm (GA) to integrate optimization capabilities into the FISs. After the GA-applied training process, the trained FISs provided near-optimal control signals in terms of energy consumption of the chaser spacecraft. However, the control signals directly obtained by the trained FISs have included undesired peaks. Therefore, this study mainly aims to identify the issues and their reasons by leveraging the FIS's interpretability. Also, the enhancement of the previously developed FIS controller is achieved by adjusting the internal parameters of the FISs.

2 Dynamic Model of Spacecraft

This study considers an RPO mission involving two spacecraft orbiting Earth, focusing specifically on the final approach phase for successful docking. In this scenario, an active spacecraft, referred to as the chaser, maneuvers towards a passive space-

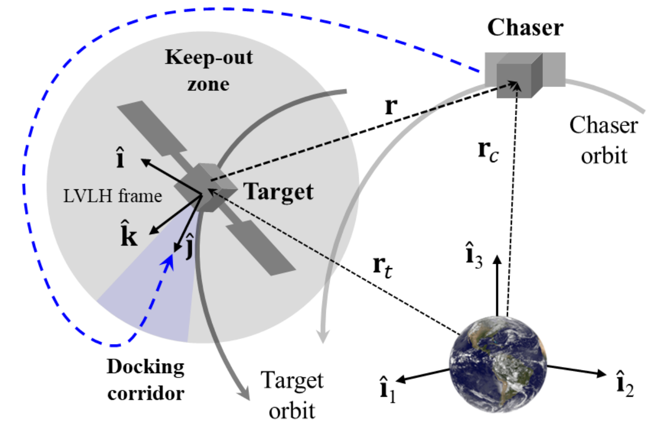

Fig. 1 Concept of the rendezvous and proximity operation

craft known as the target. Here, the target is assumed to be a cooperative spacecraft, sharing its state information with the chaser. Consequently, the chaser's relative position and velocity with respect to the target are known. To describe the chaser's translational motion relative to the target, a co-moving frame centered on the target is introduced. In this frame, the x-axis points from Earth's center to the target, while the y-axis aligns with the target's velocity vector. The z-axis is perpendicular to both the x- and y-axes, representing the direction of the angular momentum vector of the target's orbit, as illustrated in Figure 1. This co-moving reference frame serves as a local vertical/local horizontal (LVLH) frame, expressed as [7]

$$\ddot{x} - 3n^2x - 2n\dot{y} = (f_x + d_x)/m, \tag{1}$$

$$\ddot{y} + 2n\dot{x} = (f_y + d_y)/m, \tag{2}$$

$$\ddot{z} + n^2z = (f_z + d_z)/m, \tag{3}$$

where x, y, and z are the chaser's relative position for each axis with respect to the target in the LVLH frame ($\mathbf{r} = [x,\ y,\ z]^{\mathrm{T}}$), f_x, f_y, and f_z are the chaser's control force for each axis ($\mathbf{f} = [f_x,\ f_y,\ f_z]^{\mathrm{T}}$), d_x, d_y, and d_z are the disturbance force acting on the chaser ($\mathbf{d} = [d_x,\ d_y,\ d_z]^{\mathrm{T}}$), m is the mass of the chaser, and n is the angular velocity of the target (i.e., mean motion) defined as $n = \sqrt{\mu/||\mathbf{r}_t||^2}$. Here, μ is the standard gravitational parameter of the Earth, and $||\mathbf{r}_t||$ is the distance between the center of the Earth and the target. This study assumes that the chaser's attitude is already aligned with the target's attitude, allowing the focus to be solely on the chaser's translational motion.

3 FIS-Applied Control Strategy

This section introduces the physical constraints for the final approach and operational procedures of the chaser. Then, the overview of the FIS-applied control strategy and the optimization process is elaborated.

3.1 Constraints

This work employs physical constraints about the chaser and target for the safe final approach. First, the limited thrust force of the thrusters oriented along each body axis is taken into account as follows:

$$|f_i| \leq f_{\max} \ (i = x, y, \text{ and } z), \tag{4}$$

where f_i is the component of the force vector, and $f_{\max}$ is the maximum thrust force. In addition, as shown in Fig. 2, a keep-out zone around the target with a radius of r_k is defined for the chaser to avoid potential collision with the target as follows:

$$||\mathbf{r}|| > r_k, \tag{5}$$

Moreover, a docking corridor with a cone angle of β along the docking port direction is considered as

$$\hat{\mathbf{r}}_p \cdot \hat{\mathbf{r}} \geq \cos\beta, \tag{6}$$

where $\hat{\mathbf{r}}_p$ is the unit vector of the docking port direction from the target. That is, the chaser initially moves toward the entrance of the docking corridor by passing around the keep-out zone to avoid collision. Then, the chaser approaches the docking port of the target along the docking corridor.

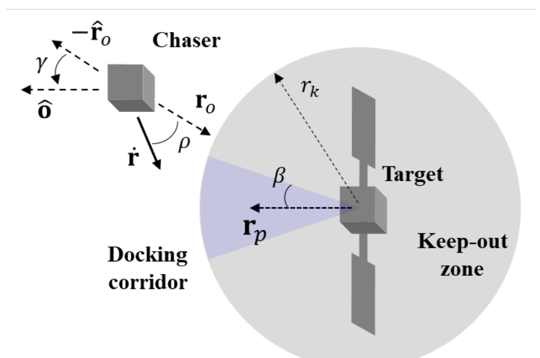

Fig. 2 Physical constraints around the target

3.2 FIS Structure and Its Optimization

The control force of the chaser is defined by $\mathbf{f} = \mathbf{f}_t + \mathbf{f}_c$, where $\mathbf{f}_t$ denotes the force allowing the chaser to approach the target and $\mathbf{f}_c$ represents the repelling force to avoid a potential collision. In this work, the component of $\mathbf{f}_t$ in each axis, denoted as $f_{t,i}$, is directly determined by FIS1, whereas FIS2 computes the magnitude of $\mathbf{f}_c$ as shown in Fig. 3. The direction of the repelling vector, illustrated in Fig. 2, is expressed as

$$\hat{\mathbf{o}} = -R\hat{\mathbf{r}}_0, \tag{7}$$

where $-\hat{\mathbf{r}}_o$ indicates the unit direction vector from the closest point between the chaser and the keep-out zone to the chaser, and R is the rotation matrix defined as [14]

$$R = \begin{bmatrix} e_1^2\kappa + \cos\gamma & e_1 e_2\kappa - e_3 \sin\gamma & e_1 e_3\kappa + e_2 \sin\gamma \\ e_2 e_1\kappa + e_3 \sin\gamma & e_2^2\kappa + \cos\gamma & e_2 e_3\kappa - e_1 \sin\gamma \\ e_3 e_1\kappa - e_2 \sin\gamma & e_3 e_2\kappa + e_1 \sin\gamma & e_3^2\kappa + \cos\gamma \end{bmatrix}. \tag{8}$$

Note that $\kappa = 1 - \cos\gamma$, and e_i for $i = 1, 2, 3$ is the element of a vector ($\mathbf{e}$) that is perpendicular to the plane formed by $\mathbf{r}_o$ and $\mathbf{r}$, which is defined by

$$\mathbf{e} = \frac{\mathbf{r}_o \times \mathbf{r}}{||\mathbf{r}_o||||\mathbf{r}||}. \tag{9}$$

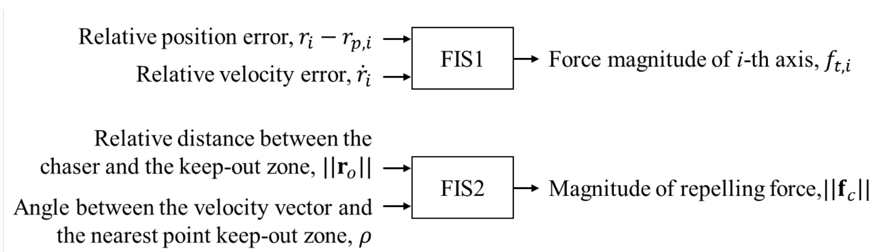

Fig. 3 Structure of two FISs

Figure 4 depicts the overall concept of the GA-applied FIS optimization process. Following this, the parameters of the membership functions (MFs) and the rules from the two FISs are extracted and fed into the GA. Subsequently, the parameters of the FISs undergo the GA's evolutionary processes, such as selection, crossover, mutation, and elitism. The parameters are then evaluated using the fitness function. In this work, the fitness function for the optimization is defined as the total control effort of the chaser including a penalty term η to discourage undesired behaviors as follows:

$$\mathcal{L}_{\text{fitness}} = \int_0^{t_f} \mathbf{f}^{\mathrm{T}}\mathbf{f}\,dt + \eta. \tag{10}$$

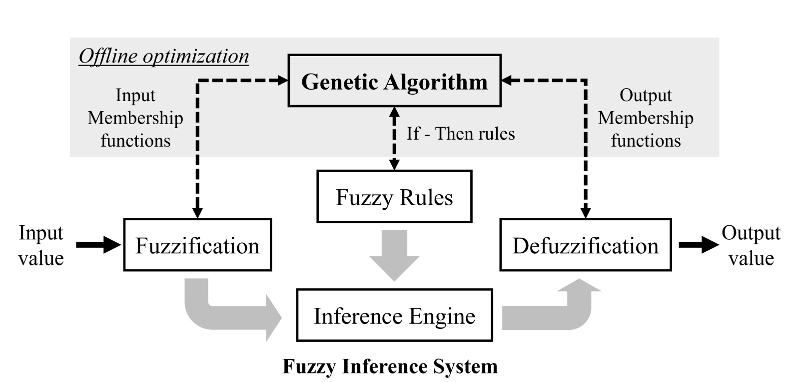

Fig. 4 Optimization of FIS aided by GA

Note that a significant penalty value is added to the fitness function if the chaser performs undesirable behavior, such as high relative position and velocity errors near the target.

4 Improvement of FIS Output

This work aims to not only identify the reasons for the issues of the previously developed approach but also resolve such issues by leveraging the FIS's interpretability. Thus, this section outlines both the identified issues and their underlying causes in the preliminary results, as well as the methods employed to resolve these issues and enhance the performance of FISs.

In the author's preliminary work [5], the proposed control approach was validated through numerical simulations using the simulation parameters tabulated in Table 1. In the training process, four different scenarios were taken into account using various initial relative positions in the LVLH frame (x : ± 80 m, y : 90 m, and z : ± 70 m). Note that the positive initial relative position in the y-axis was set because the docking port is aligned with the positive y-direction. In addition, a large penalty value in the fitness function was applied when one violates two conditions: i) the average of the norm of the relative position error during the last 30 seconds is less than 0.5 m, and ii) the average of the norm of the relative velocity error during the last 30 seconds is less than 0.05 m/s. The previously trained results and the improved results for one of the training scenarios are illustrated in Fig. 5. Note that the previous and improved results are displayed side by side for easy comparison between the results. Moreover, the FIS1's previous and improved MFs are illustrated in Fig. 6. Note that the linguistic variables "LN", "SN", "Z", "SP", and "LP" represent "Large Negative", "Small Negative", "Zero", "Small Positive", and "Large Positive", respectively.

Table 1 Simulation parameters for spacecraft and GA [5]

	Parameters	Values
Spacecraft-related	Simulation time (t_f)	300 (s)
	Time interval (dt)	0.1 (s)
	Chaser's mass (m)	100 (kg)
	Maximum force ($f_{\max}$)	10 (N)
	Cone half-angle (β)	30 (deg)
	Rotation angle (γ)	45(deg)
	Radius of keep-out zone (r_k)	18 (m)
	Relative distance between the target and the center of the Earth (r_t)	6878 (km)
GA-related	Maximum generations	1000
	Population size	20
	Stall generations	200
	Selection algorithm	Tournament selection
	Tournament size	4
	Crossover algorithm	Scattered crossover
	Mutation algorithm	Adaptive feasible
	Elitism ratio	0.05

In the previously trained results in Fig. 5(e), undesired behavior was observed in the control force trajectory, especially from $\mathbf{f}_t$. For this reason, this work mainly concentrates on dealing with $\mathbf{f}_t$-related FIS, which is FIS1, in order to not only identify the issues causing such undesired behavior (a sudden peak of the control force) but also address the issues by leveraging the FIS's interpretability.

In Fig. 5(e), the control force trajectory f_y includes sudden changes from 4.6 N to -1.6 N around 108 seconds. This change is observed in the defuzzified output of FIS1 around this time frame due to the left trapezoidal shape of each aggregated output, as shown in Fig. 7. Moreover, looking at Fig. 8, it is found that a large change in the degree of membership of "LN" of the output MF among the activated rules, highlighted in blue, causes this undesired behavior.

Such a sudden change might be caused by the change in the input for the relative position error because the desired relative position rapidly shifts from the intermediate position around the docking corridor entrance to the docking port of the target. For this reason, the desired relative position around the docking corridor is modified to smoothly transition to the final docking port.

Also, in the preliminary work, FIS1 is commonly used to compute the force component of each axis. However, the chaser's motion in each axis governed by Eqs. (1)–(3) is coupled to each other, especially for the x- and y- axis ($\hat{\mathbf{i}}$ and $\hat{\mathbf{j}}$). Therefore, this work utilizes one more FIS (referred to as FIS3) for generating the control force in the y-axis only. That is, FIS1 determines the x- and z-axis control forces while FIS3 determines the y-axis control force. This could allow FIS3 to compute the control force effectively and independently.

Despite smooth changes in the desired relative position and the independent FIS for the y-axis force, quick changes in the control force still occur because the

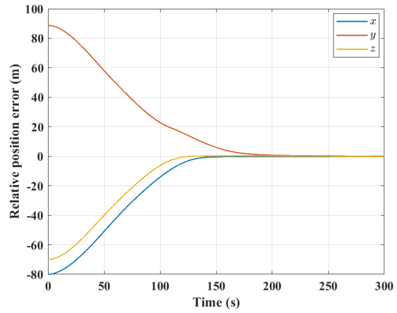

(a) Relative position error (previously trained)

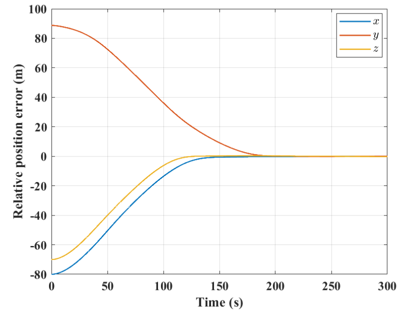

(b) Relative position error (retrained)

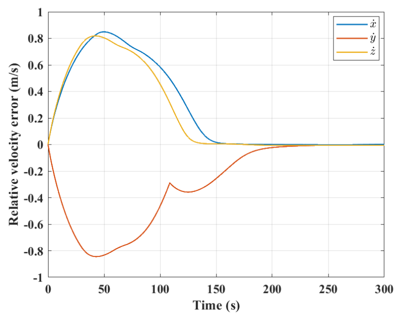

(c) Relative velocity error (previously trained)

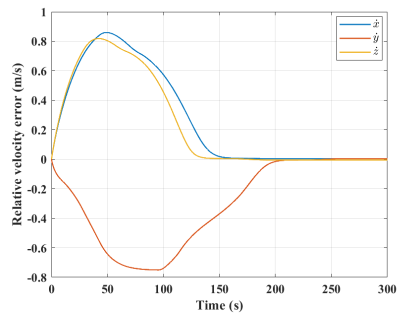

(d) Relative velocity error (retrained)

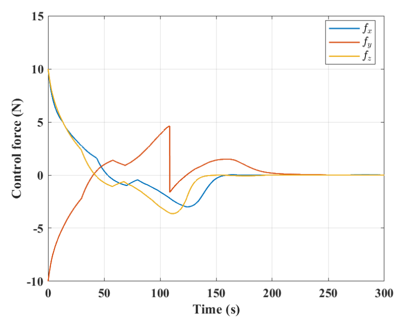

(e) Force (previously trained)

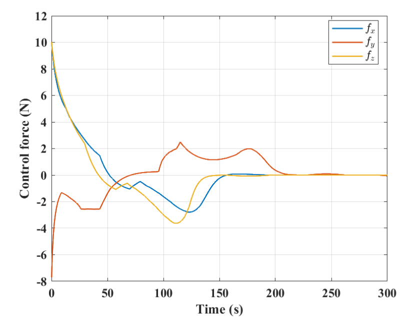

(f) Force (retrained)

Fig. 5 Chaser's states (previously trained and retrained)

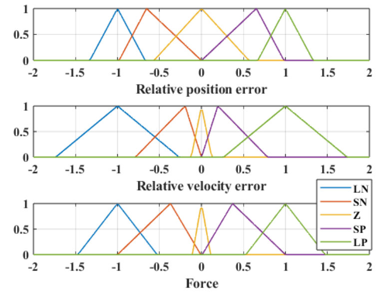

(a) Input and output MFs (previously trained)

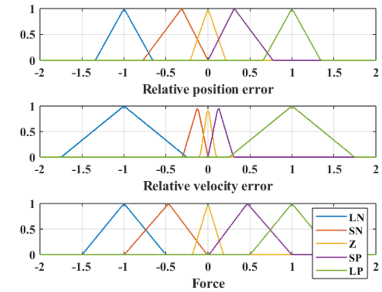

(b) Input and output MFs (retrained)

Fig. 6 MFs for the y-axis force generation

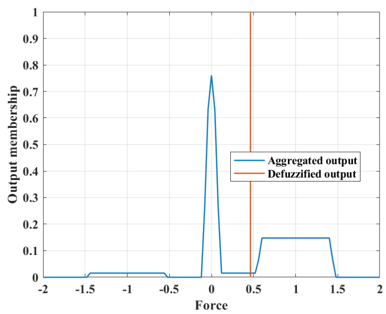

(a) At 108.6 seconds

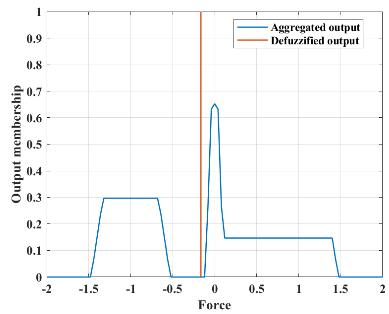

(b) At 108.7 seconds

Fig. 7 Aggregated and defuzzified output of FIS1

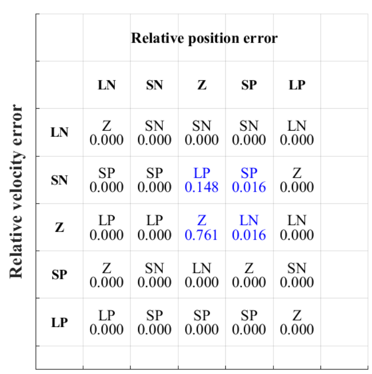

(a) At 108.6 seconds

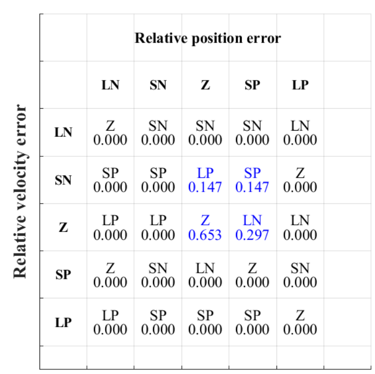

(b) At 108.7 seconds

Fig. 8 Activated rules of FIS1

FIS3 based on the trained FIS1 is not optimized for the current revision. Therefore, additional training for FIS3 only is conducted to improve the performance of FIS3. For the retraining, the same simulation parameters for the chaser and the GA in Table 1 are utilized.

After retraining, the MFs' shape of FIS3 is changed as shown in Fig.6(b) whereas the rules remain the same. Also, the results using the retrained FIS3 displayed on the right side of Fig. 5 show that the trajectories for the relative position and velocity errors have become smoother compared to the results shown on the left side of Fig. 5.

In the control force trajectory, although the trajectory is not as smooth as the other axes, a sudden sign change shown in the previously trained results is eliminated, and the total control effort (fitness value) of this scenario is also reduced from 3838 (preliminary work) to 3026. Also, it is observed that the time derivative of the control force in the retrained results overall does not exceed 0.4 N/s, unlike the previously trained results whose maximum is over 60 N/s. To further improve the output of FIS3 for generating a more natural and smooth control force trajectory, adjusting the FIS parameters manually and/or retraining the FISs with a different fitness function could be applicable.

5 Conclusions

In the author's previous work, one proposed a fuzzy inference system (FIS)-applied control strategy for safe rendezvous and proximity operation of a chaser while minimizing the control effort. The main focus of this work is to unveil the cause of the undesired behavior observed in the previous work as well as improve the previously developed FIS controller by exploiting the interpretability of the FIS. After identifying the reasons for a sudden change in the control force generated by the FIS, the proper adjustment of the control strategy, like employing and retraining an independent FIS for handling the coupled dynamics, is conducted. Consequently, the results demonstrate the retrained FIS produces the proper control force without a sudden change as well as further minimizes the control effort. In future work, the smoothness of the output of the FIS will be improved by retraining the FIS with a different fitness function and manually exploring the FIS parameters.

References

1. Brandonisio, A., Capra, L., Lavagna, M.: Deep reinforcement learning spacecraft guidance with state uncertainty for autonomous shape reconstruction of uncooperative target. Advances in Space Research (2023). DOI https://doi.org/10.1016/j.asr.2023.07.007
2. Cao, L., Qiao, D., Xu, J.: Suboptimal artificial potential function sliding mode control for spacecraft rendezvous with obstacle avoidance. Acta Astronautica **143**, 133–146 (2018). DOI https://doi.org/10.1016/j.actaastro.2017.11.022

3. Choi, D., Chhabra, A., Kim, D.: Genetic algorithm-aided fuzzy controller for spacecraft attitude maneuver with uncertainties. In: ASCEND 2021, pp. 1–13. AIAA (2021). DOI 10.2514/6.2021-4174
4. Choi, D., Chhabra, A., Kim, D.: Intelligent cooperative collision avoidance via fuzzy potential fields. Robotica p. 1–20 (2021). DOI 10.1017/S0263574721001454
5. Choi, D., Chhabra, A., Kim, D.: Fuzzy inference system-applied spacecraft control for final approach of rendezvous process. In: 2023 23rd International Conference on Control, Automation and Systems (ICCAS), pp. 1401–1406 (2023). DOI 10.23919/ICCAS59377.2023.10316839
6. Choi, D., Kim, D.: Intelligent multi-robot system for collaborative object transportation tasks in rough terrains. Electronics **10**(12) (2021). DOI 10.3390/electronics10121499
7. Clohessy, W.H., Wiltshire, R.S.: Terminal guidance system for satellite rendezvous. Journal of the Aerospace Sciences **27**(9), 653–658 (1960). DOI 10.2514/8.8704
8. Federici, L., Benedikter, B., Zavoli, A.: Deep learning techniques for autonomous spacecraft guidance during proximity operations. Journal of Spacecraft and Rockets **58**(6), 1774–1785 (2021). DOI 10.2514/1.A35076
9. Guang, Z., Heming, Z., Liang, B.: Attitude dynamics of spacecraft with time-varying inertia during on-orbit refueling. Journal of Guidance, Control, and Dynamics **41**(8), 1744–1754 (2018). DOI 10.2514/1.G003474
10. Li, Q., Yuan, J., Zhang, B., Wang, H.: Artificial potential field based robust adaptive control for spacecraft rendezvous and docking under motion constraint. ISA Transactions **95**, 173–184 (2019). DOI https://doi.org/10.1016/j.isatra.2019.05.018
11. Li, X., Zhu, Z., Song, S.: Non-cooperative autonomous rendezvous and docking using artificial potentials and sliding mode control. Proceedings of the Institution of Mechanical Engineers, Part G: Journal of Aerospace Engineering **233**(4), 1171–1184 (2019). DOI 10.1177/0954410017748988
12. Mancini, M., Bloise, N., Capello, E., Punta, E.: Sliding mode control techniques and artificial potential field for dynamic collision avoidance in rendezvous maneuvers. IEEE Control Systems Letters **4**(2), 313–318 (2020). DOI 10.1109/LCSYS.2019.2926053
13. Oestreich, C.E., Linares, R., Gondhalekar, R.: Autonomous six-degree-of-freedom spacecraft docking with rotating targets via reinforcement learning. Journal of Aerospace Information Systems **18**(7), 417–428 (2021). DOI 10.2514/1.I010914
14. Schaub, H., Junkins, J.: Analytical Mechanics of Space Systems. AIAA education series. American Institute of Aeronautics and Astronautics (2003)
15. Shi, L., Katupitiya, J., Kinkaid, N.M.: Hybrid control of space robot in on-orbit screw-driving operation. IEEE Transactions on Aerospace and Electronic Systems **54**(3) (2018). DOI 10.1109/TAES.2017.2780558